Proposed extension of double-ended gauge block interferometers for measuring spheres

OPEN ACCESS
IOP Publishing
Measurement Science and Technology
Meas. Sci. Technol. **32** (2021) 084010 (11pp)
https://doi.org/10.1088/1361-6501/abfe35

Proposed extension of double-ended gauge block interferometers for measuring spheres

René Schödel* and **Markus Fischedick**

Physikalisch-Technische Bundesanstalt (PTB), Bundesallee 100, 38116 Braunschweig, Germany

E-mail: rene.schoedel@ptb.de

Received 26 January 2021, revised 22 April 2021
Accepted for publication 5 May 2021
Published 18 May 2021

Abstract

Double-ended gauge block interferometers (DEI) are becoming more and more established. This paper suggests its extension for enabling interferometric measurement of diameter topographies of spheres as an alternative to the existing spherical Fizeau interferometers. The extension essentially consists in the addition of two lenses which are as similar as possible, which are arranged symmetrically around the sphere to be measured. The determination of the diameter topography from the interferometric measurements with inserted and without sphere in the extended DEI is derived and specific aspects are discussed. An adjustment strategy for the extended DEI is also suggested. In conclusion, the proposed extension appears to be a promising measurement tool, especially for measuring small spheres, as required for applications in coordinate metrology.

Keywords: double-ended interferometer, gauge blocks, spheres, length measurement, interferometry

(Some figures may appear in colour only in the online journal)

1. Introduction

Industry and technology depend on precise length measurements. Their connection to the international length scale is essentially ensured by interferometric measuring methods [1], which are constantly being further developed for this reason. In order to ensure the traceability of the length to the SI definition, gauge blocks play an important role. Over the past two decades, more and more double-ended gauge block interferometers (DEI) have been developed [2–6]. They offer an alternative to get traceable measurements of the absolute length of gauge blocks without having to wring them onto a platen. The measurement principle and some history of the DEI is described in [3]. Besides gauge blocks, measurement of spheres is increasingly desired by industry. As an example, a stakeholder workshop with experts from industry and academia with a background on metrology requirements from manufacturing, held at PTB in March 2020, came to the conclusion that there is an important and urgent need for the characterization of spheres with diameters from 1 mm to 45 mm on an uncertainty level of approximately 10 nm for applications in coordinate metrology.

The idea of measuring spheres interferometrically originated in the search for most precise volume measurements (see [7, 8] and references therein). An exact measurement of the sphere volume requires, on the one hand, the existence of high-quality spheres. In 1987, Leistner [9] initially produced a 1 kg silicon sphere ($d \approx 93.7$ mm) with an exceptionally high optical quality. On the other hand, to determine the volume of

* Author to whom any correspondence should be addressed.

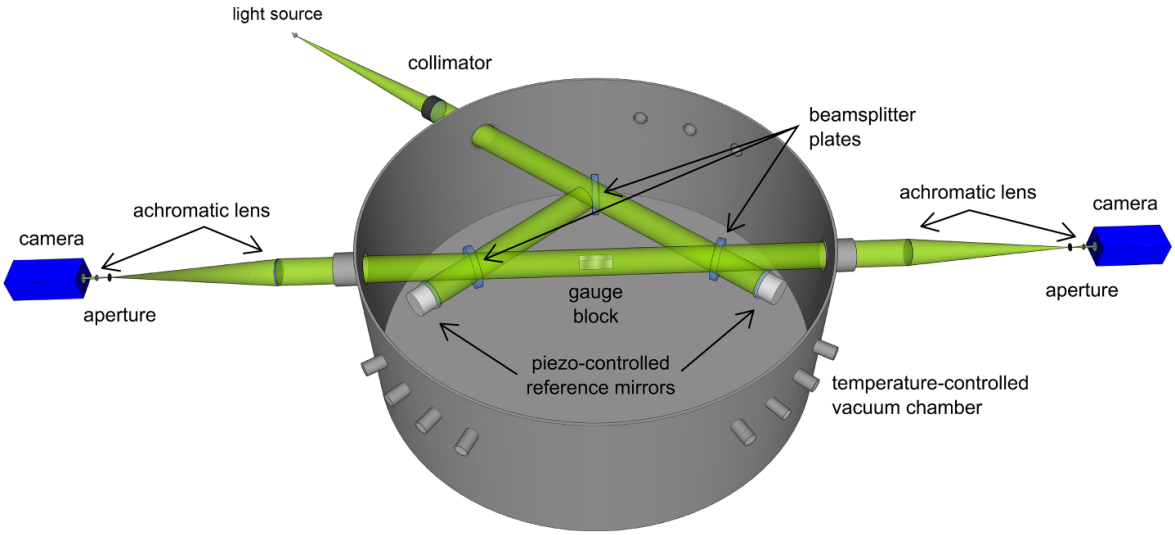

Figure 1. Structure of PTB's DEI as it was originally designed for measuring prismatic bodies.

such a sphere at a relative level of 10^{-7}, the mean diameter must be measured at an uncertainty level of 1 nm. Even spheres of the highest possible manufacturing quality show diameter variations above 20 nm. The determination of the mean diameter therefore requires the measurement of numerous diameters with orientations covering the entire surface of a sphere. The Fizeau type interferometer proposed by Sounders [7] can measure the diameter of a sphere along the optical axis. Such interferometer, equipped with a refined angular positioning unit, was established at NMIJ [10]. In 1997 a spherical Fizeau interferometer was proposed, designed, built and established at PTB, which allows a diameter topography of a sphere to be measured in a relatively large solid angle range around the optical axes [11, 12]. Later a second spherical Fizeau interferometer was also built at PTB, which has a significantly different geometry [13]. These unique spherical Fizeau interferometers have evolved into the most accurate volumetric instruments over the past two decades. The main driver of this development was the Avogadro project, which ended with the fixing of the numerical value of the Avogadro constant or the related Planck constant and the redefinition of the kilogram in 2019 [14]. With the achieved relative standard measurement uncertainty of 7×10^{-9} for the volume of large (94 mm) spheres, or 0.1 nm for the mean spherical radius, PTB's spherical interferometry is far beyond all measurement options established in dimensional metrology, especially when it comes to commercial devices. Today, these two spherical Fizeau interferometers are in a quasi-continuous measuring operation for the primary realization of the mass according to the new International System of Units [15].

This paper suggests an alternative approach for measuring spheres which is based on the extension of an existing DEI. The extension consists in adding two lenses which are as similar as possible and which are arranged symmetrically around the sphere to be measured. The following section begins with a brief description of PTB's DEI in its present status, followed by an illustration of the proposed extension for the measurement of diameter topographies of spheres.

2. Original design of PTB's double-ended interferometer

Figure 1 illustrates the PTB's DEI as it was originally set up for measuring prismatic bodies [16, 17]. The main part is situated in a temperature-controlled vacuum chamber which has a diameter of 1.4 m. The core component of the interferometer consists of a triangular array of beam splitter plates with a diameter of 130 mm and a thickness of 20 mm. The flatness of the semi-reflecting chromium coated surfaces of these plates is better than 15 nm (PV) and the reverse side has an anti-reflective coating (99.9%). There is a 10 arc minute wedge angle between both sides to change the direction of remaining unwanted reflections. The light source is represented by the end of a fibre that is designed for the best possible transmission of the two successively used wavelengths 532 nm and 633 nm of iodine-stabilized lasers. After collimation ($f_{\mathrm{coll}} = 500$mm), the diameter of the beam bundle of almost uniform light intensity passing through the interferometer is approximately 80 mm. The reference mirrors with a diameter of 80 mm and a flatness of better than 20 nm (PV) are mounted on three-axes piezo actuators, which allow the mirrors to be moved for phase shifting and to tilt the mirrors in both axes. In the middle between the two lower beam splitter plates is a motorized adjustment table on which the prismatic body (e.g. a gauge block) to be measured is located. The imaging arms with a quasi-telecentric beam path are located on each side of the interferometer output. Each arm consists of an achromatic focusing lens, an aperture diaphragm in its focus that stops unwanted reflections, and a second achromatic lens.

The cameras are each mounted on a translation stage in order to enable a sharp image of the end face of the prismatic body to be set on the CCD chip. In order to ensure that the light rays hit the front surfaces of the prismatic body perpendicularly, the reference mirrors are first aligned in a way that the reflection is returned exactly to the light source (autocollimation). Then the beam splitters are adjusted so that the number of interference fringes is reduced to nearly

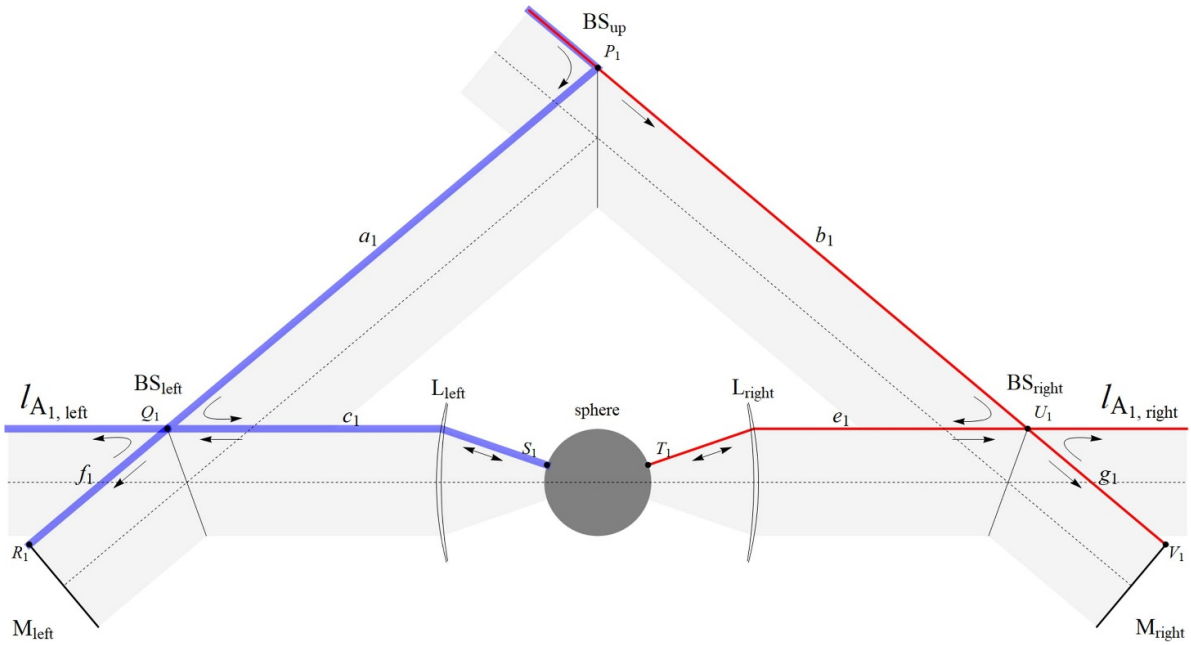

Figure 2. Scheme for the double-end interferometer, which is extended by two lenses, L_{left} and L_{right}, for measuring spheres. The case is shown where the sphere is placed in the centre of the two lenses. An incident partial beam from the collimated bundle (marked in grey) travels through points marked with index '1'. The dotted line indicates the central axis of the beam bundle.

zero. Crosshairs positioned after the collimator can be used to ensure that the beams passing through the two interferometer arms are not shifted towards each other. After adjusting the light rays that pass the prismatic body, the latter is adjusted so that the front faces visible in each centre of the two interference images appear almost without fringes, which of course is limited by the quality of the parallelism of the body.

The DEI is in a ready-to-measure state and is being systematically examined at PTB regarding the achievable measurement uncertainty and necessary corrections [18].

3. Proposed extension and derivation of the diameter topography for the DEI

Figure 2 shows a scheme for the double-ended interferometer, which is extended by two identical lenses[1], L_{left} and L_{right}, for measuring spheres. The lenses are separated from each other by twice their focal length and the sphere is ideally positioned exactly in the middle between them at the focal point. The collimated beam bundle is marked in grey. The incident partial beam is split at the Point P_1 of the upper beam splitter, BS_{up}, reflected at Q_1 or U_1 further travelling the measuring pathway either from Q_1 via L_{left} to S_1 or from U_1 via L_{right} to T_1 on the sphere where they are retro-reflected in each case. Part of beams transmitting either through beam splitter BS_{left} or BS_{right} travel the respective reference pathway from Q_1 to R_1 (left) or from U_1 to V_1 (right), being retro- reflected at the reference mirror and then reflected at Q_1 (left) or U_1 (right). From there these beams take the same path as the respective beams that are retro reflected on the sphere.

Thus, two-beam interference occurs on each side of the interferometer output from which the lengths $l_{A_1,\,left}$ and $l_{A_1,\,right}$, each referring to the length differences between the measuring and the reference pathways, can be determined:

$$l_{A_1,\,left} = a_1 + 2\cdot c_1 - (a_1 + 2\cdot f_1) = 2\cdot(c_1 - f_1) \qquad (1)$$

$$l_{A_1,\,right} = b_1 + 2\cdot e_1 - (b_1 + 2\cdot g_1) = 2\cdot(e_1 - g_1)\,, \qquad (2)$$

in which $a_1 = \overline{P_1Q_1}$, $b_1 = \overline{P_1U_1}$, $c_1 = \widetilde{Q_1S_1}$, $e_1 = \widetilde{T_1U_1}$, $f_1 = \overline{Q_1R_1}$ and $g_1 = \overline{U_1V_1}$.

The situation is the same for figure 3, i.e. for the index '2' of the points, based on:

$$l_{A_2,\,left} = a_2 + 2\cdot c_2 - (a_2 + 2\cdot f_2) = 2\cdot(c_2 - f_2) \qquad (3)$$

$$l_{A_2,\,right} = b_2 + 2\cdot e_2 - (b_2 + 2\cdot g_2) = 2\cdot(e_2 - g_2)\,, \qquad (4)$$

in which $a_2 = \overline{P_2Q_2}$, $b_2 = \overline{P_2U_2}$, $c_2 = \widetilde{Q_2S_2}$, $e_2 = \widetilde{T_2U_2}$, $f_2 = \overline{Q_2R_2}$ and $g_2 = \overline{U_2V_2}$.

Figures 4 and 5 show the case of the extended DEI without an inserted sphere. The blue-marked incident partial beam in figure 4, travels from O_1 to P_1 to Q_1, and then along the measuring path from left to the right over L_{left}, S_1 and T_2 and over L_{right} to U_2. From there, this beam will interfere with the red-marked beam, which travels the reference pathway on the right side over O_2, P_2, U_2, V_2 and U_2. Thus, for the situation shown

[1] In principle, the lenses could have different focal lengths, but this would make converting the results to spherical coordinates unnecessarily complex.

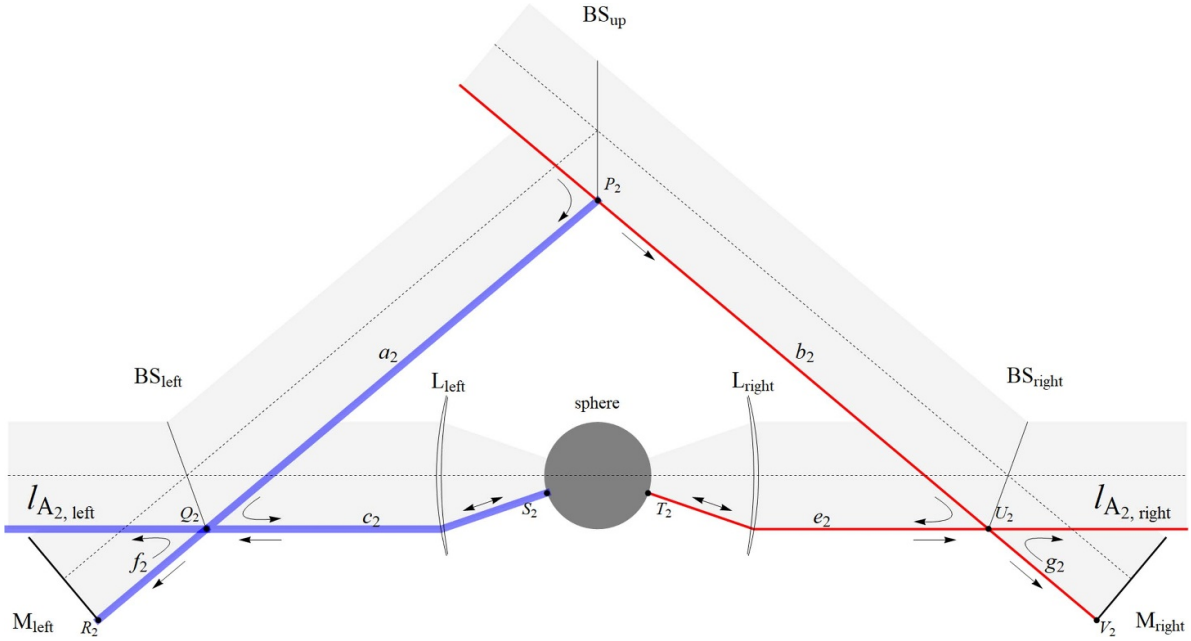

Figure 3. Scheme for the double-end interferometer, which is extended by two lenses for measuring spheres. The case is shown where the sphere is placed in the centre of the two lenses. An incident partial beam from the collimated bundle (marked in grey) travels through points marked with index '2'.

in figure 4, the two-beam interference on the right side of the empty interferometer is related to the length difference:

$$l_{B_2,\,right} = h_1 + a_1 + c_1 + d_{12} + e_2 - (h_2 + b_2 + 2\cdot g_2)\,, \quad (5)$$

in which $h_1 = \overline{O_1P_1}$, $h_2 = \overline{O_2P_2}$ and $d_{12} = \overline{S_1T_2}$ represents the diameter of the removed sphere for the given orientation.

Similarly, the red-marked incident partial beam in figure 4, which travels from O_2 to P_2 and U_2, and then along the measuring pathway from right to left via L$_{right}$, T_2 and S_1 and via L$_{left}$ to Q_1. From there, this beam will interfere with the blue marked beam, which travels the reference pathway on the left side over O_1, P_1, Q_1, R_1 and Q_1. Thus, for the situation shown in figure 4, the two-beam interference on the left side of the empty interferometer is related to the length difference:

$$l_{B_1,\,left} = h_2 + b_2 + e_2 + d_{12} + c_1 - (h_1 + a_1 + 2\cdot f_1)\,. \quad (6)$$

In the same way, the blue-marked incident partial beam in figure 5 causes the two-beam interference on the right-hand side of the empty interferometer, which is related to the length difference:

$$l_{B_1,\,right} = h_2 + a_2 + c_2 + d_{21} + e_1 - (h_1 + b_1 + 2\cdot g_1)\,, \quad (7)$$

where $d_{21} = \overline{S_2T_1}$ represents the diameter of the removed sphere for the given orientation.

Similarly, the red-marked incident partial beam in figure 5 causes the two-beam interference on the left side of the empty interferometer, which is related to the length difference:

$$l_{B_2,\,left} = h_1 + b_1 + e_1 + d_{21} + c_2 - (h_2 + a_2 + 2\cdot f_2)\,. \quad (8)$$

Fortunately, the quantities $a_1, a_2, b_1, b_2, c_1, c_2, e_1, e_2, f_1, f_2$, g_1, g_2, h_1, h_2 can be eliminated from the equations (1) to (8), resulting in the two simple equations for the diameters d_{12} and d_{21}:

$$d_{12} = \frac{1}{2}\left(l_{B_1,\,left} + l_{B_2,\,right} - l_{A_1,\,left} - l_{A_2,\,right}\right), \quad (9a)$$

and

$$d_{21} = \tfrac{1}{2}\left(l_{B_2,\,left} + l_{B_1,\,right} - l_{A_2,\,left} - l_{A_1,\,right}\right). \quad (9b)$$

In the figures 2–5, the beams marked with the index '1' are arranged point-symmetrically around the optical axis to the beams marked with the index '2'. Consequently, the lateral coordinates of lengths $l_{A\,/\,B,\,left\,/\,right}$ identified with the index '1' in equation (9) correspond to the point-reflected coordinates identified with the index '2'. Therefore, equation (9) can be put into a general form for each partial beam from the beam bundle:

$$d(x,y) = \tfrac{1}{2}\left[l_{B,\,left}(x,y) + l_{B,\,right}(x',y') - l_{A,\,left}(x,y) - l_{A,\,right}(x',y')\right], \quad (10)$$

where (x,y) denotes the lateral coordinates within the collimated beam bundle and (x',y') their mathematical reflection at the point (x_c,y_c) on the optical axis, i.e.

$$(x',y') = (x_c,y_c) - (x - x_c, y - y_c) = (2x_c - x, 2y_c - y)\,. \quad (11)$$

The (x,y) coordinates of the diameter topography are then converted into angular coordinates, taking into account the focal length of the lenses between which the sphere is located.

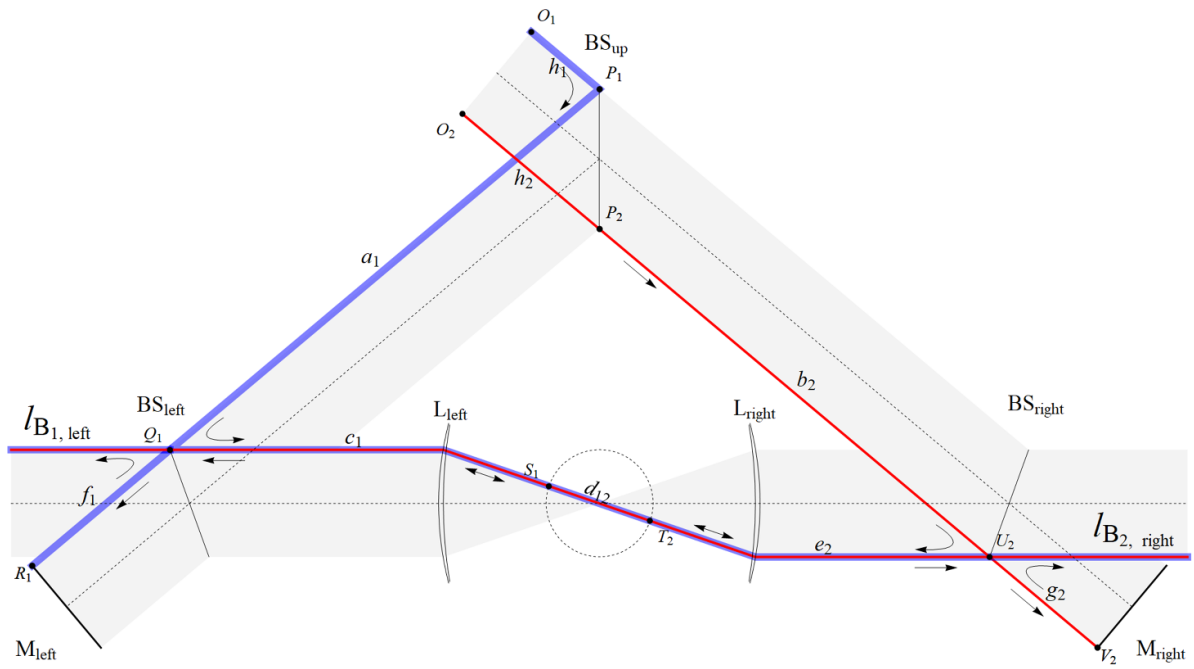

Figure 4. The extended DEI without the sphere. The interference at both sides requires two separate partial beams from the collimated bundle (marked in grey).

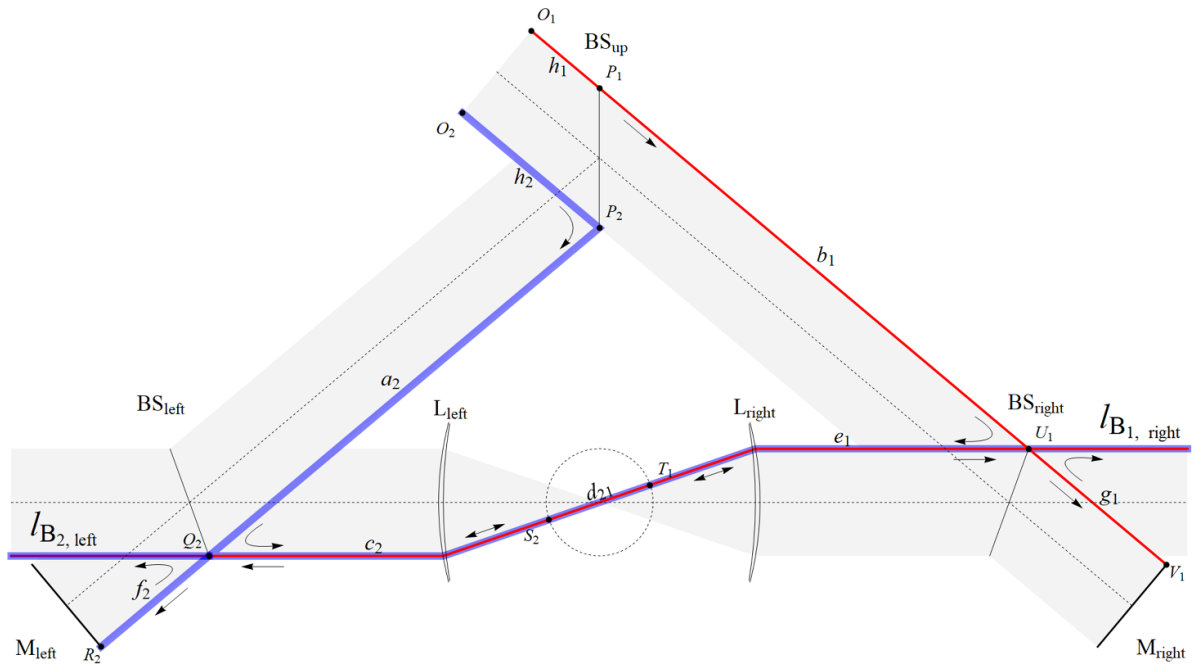

Figure 5. The extended DEI without the sphere. The interference at both sides requires two separate partial beams from the collimated bundle (marked in grey).

4. Aspects of the extended DEI

4.1. Light sources and application of phase stepping interferometry

The first advantage of extending PTB's DEI is the possibility of using the two widely different laser wavelengths 532 nm and 633 nm—in contrast to the strict limitation of 633 nm with the PTB's spherical Fizeau interferometers. This enables the use of coincidence methods [19], which significantly expand the unambiguity range of an interferential length measurement. This is particularly important for small spheres made of different materials, the estimated diameter of which cannot be determined with sufficient accuracy from the values of density and mass. The second advantage of the DEI extension is the way in which phase steps can be generated

between the recorded interferograms, as is necessary for the phase calculation using phase stepping interferometry. With the spherical Fizeau interferometers, due to the spherical reference surfaces the phase stepping can only be introduced by defined shifts of the light frequency. This approach also modulates any parasitic interference, which, if not counteracted, causes errors in the resulting phase topography. In contrast to this, the phase stepping interferometry in the DEI can be made by small shifts of the two reference mirrors within the interferometer. All interfering reflections arising outside the DEI, e.g. on the camera windows, produce visible fringe structures in the individual recorded interferograms, but are not present in the calculated phase topography. The effect of dispersion of the wedge-shaped beam splitters and the secondary reflections can be considered negligible for the selected configuration in the DEI (see [17], configuration 5 shown in table 5.1 on p 83 and corresponding effect in table 5.4. on p 90).

4.2. Involved path lengths

The general advantage of Fizeau-type interferometers is that interference occurs between two closely spaced parts, i.e. either between the sphere and a spherical reference surface or between the two spherical reference surfaces. In contrast, measurements with the extended DEI are based on the interference between light waves that have travelled relatively long distances. This concerns on the one hand the measurements with the inserted sphere (mode A, equations (1)–(4)) and the measurements in the empty interferometer (mode B, equations (5)–(8) and makes the DEI more sensitive to parameters influencing the stability of path lengths. This major weakness of the DEI must be counteracted by suitable construction, such as the use of thermally low-expansion materials and temperature stabilization through insulation, as it was made with PTB's DEI [16].

4.3. Influence of the lenses

In contrast to the spherical Fizeau interferometers, the lenses in whose focal point the centre of the sphere is located do not contain a reference surface. This fact considerably reduces the requirements for the dimensional accuracy specification of the lenses for the DEI. The focal length of the lenses must be large enough to allow sufficient space for the necessary adjustment elements. On the other hand, an optical design of the lenses must be chosen that avoids reflections on lens surfaces propagating in the same direction as the transmitted light, which would lead to parasitic interference.

From a practical point of view, it is worth considering the necessary degrees of freedom of the extensions that must be designed to be adjustable. It is clear that the sphere in any spherical interferometer must be adjustable in x, y, z and in ϑ, φ. In the spherical Fizeau interferometers, the lenses contain the reference surface for the interference, which must therefore be adjustable on the nm-scale. In contrast, the lenses of the extended DEI do not contain any reference surfaces, which fundamentally reduces the adjustment requirements. While these lenses must also be designed to move in and out of the beam, they may need to be primary laterally adjustable and the distance between them must be adjustable. However, it should be taken into account that when a lens is tilted by the angle α with respect to the centre beam axis, as shown in figure 6, the effective focal length in the plane direction is increased. In contrast, the effective focal length does not increase perpendicular to the plane shown in figure 6. Because of the resulting astigmatism, the inclination of the two lenses cannot be compensated for by increasing the distance between them. As practical matter, it may be desired to have a design without motorized adjustment of the lenses, as this would simplify the mechanics for moving the lenses into and out of the beam.

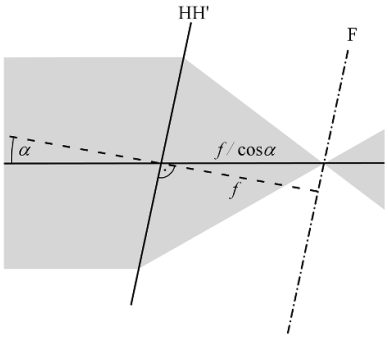

Figure 6. A parallel beam bundle passing through a lens whose axis HH'is inclined at the angle α with respect to the central beam axes. The resulting spot appears on the central axes at a distance $f/\cos\alpha$ from the lens.

Figure 7 shows first experimental investigations with PTB's DEI with inserted lenses. For this purpose, two identical achromatic lenses (Linos cage system, $f = 80$ mm) were placed on the DEI's angle-adjustable sample stage, with the distance between them being adjustable.

While the adjustment seems not to be perfect[2], it can be seen in figure 7 that the phase topographies (left and right) in the areas of the lenses show surprisingly good rotational symmetry. Visible deviations from constant phase values are caused by spherical aberration of these simple lenses. Figure 8 shows simulations with Zemax®. In figure 8, left, assuming that light passes through two simple plano-convex lenses (Thorlabs LA1608, $f = 75$ mm) the result is similar to figure 7. Figure 8, right, shows the same simulation for aspherical lenses (Thorlabs, ASL10142, $f = 79$ mm) which gives a much better result.

For the planned extension of the DEI to measure spheres, it may be necessary to have special lenses made that have similarly small errors at larger diameters as in figure 8, right.

4.4. Influence of wavefront distortion

Another aspect of the extended DEI concerns the shape and progression of the incident wave fronts, which in reality are not

[2] The wrapped phase topography in figure 7, right, has been computationally tilted slightly to show the maximum symmetry in the area of the lenses, causing the visible tilt in the area outside the lenses.

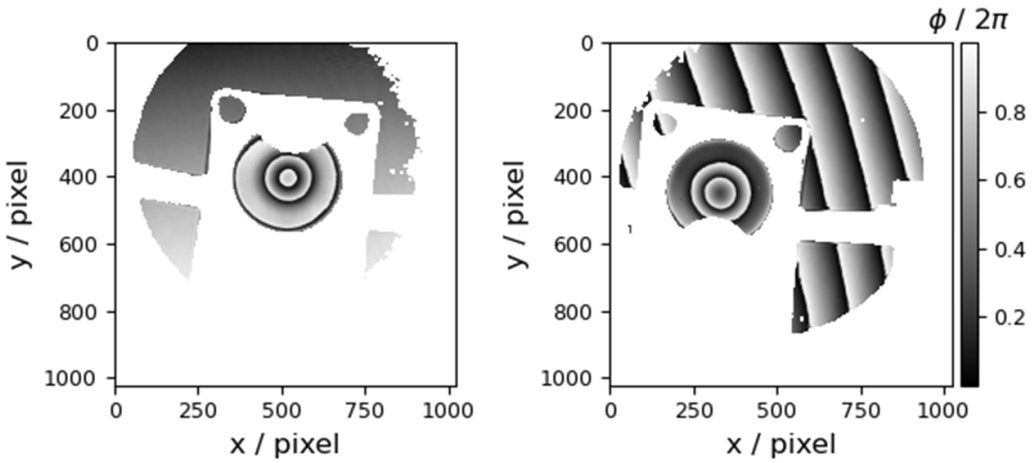

Figure 7. Wrapped phase topographies for the wavelength 532 nm obtained on the left and right side of the DEI when using simple achromatic lenses.

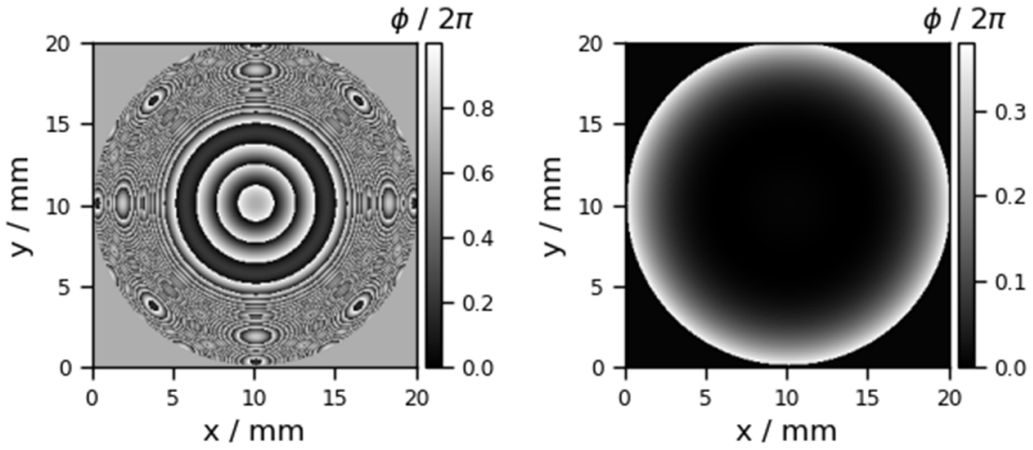

Figure 8. Simulated phase topographies using Zemax® assuming that light passes through left: two simple plano-convex lenses (Thorlabs LA1608, $f = 75$ mm) right: two aspherical lenses (Thorlabs, ASL10142, $f = 79$ mm).

ideally flat. To illustrate this effect figure 9 shows the propagation of a fictitious wavefront (I) in the extended DEI when a sphere is present. It is assumed that this wavefront is ideally flat in half a section of the beam bundle and distorted in the other half. After being split at the upper beam splitter (II), the wavefronts are reflected on the left/right beam splitter and directed to the sphere (III). The wave component passing on the left/right beamsplitter is retroreflected at the respective reference mirror and guided to the exit by reflection on the left/right beamsplitter (IV). The wave components that are reflected on the sphere pass through the respective beamsplitter on their way to the exit on the left/right side of the DEI (V_A). Consequently, at each exit of the DEI, the effect of wavefront distortion to the lengths differences $l_{\mathrm{A,\,left}}(x,y)$ and $l_{\mathrm{A,\,right}}(x,y)$ almost vanishes, apart from the unknown evolution of the distorted wavefronts due to the different light travelling distances in either the reference path or the measuring path. The situation is different for the extended DEI without sphere, as shown in figure 10. There the wave components reflected on the left/right beamsplitter (III) travel from left to right/right to left through the two lenses. Therefore, the respective wavefronts V_B that reach the exit appear point-reflected to the central axis, unlike in the cases of V_A (see figure 9 for comparison).

In order to evaluate the effect of wavefront distortion δ_wf on the measured sphere diameter, equation (10) is used in an analogous manner for the wavefronts under consideration resulting in:

$$\begin{aligned}\delta_\mathrm{wf} &= \tfrac{1}{2}\Big[(V_\mathrm{B}-\mathrm{IV})_\mathrm{left}+(V_\mathrm{B}-\mathrm{IV})'_\mathrm{right}-(V_\mathrm{A}-\mathrm{IV})_\mathrm{left}\\ &\quad -(V_\mathrm{A}-\mathrm{IV})'_\mathrm{right}\Big]\\ &= \tfrac{1}{2}\Big[\underbrace{V_\mathrm{B,\,left}-V'_\mathrm{A,\,right}}_{\approx 0}+\underbrace{V'_\mathrm{B,\,right}-V_\mathrm{A,\,left}}_{\approx 0}\Big],\end{aligned} \tag{12}$$

where the operator " ′ " again denotes mathematical point reflection around the central axis. Since the wavefronts V_B are almost identical to the point-reflected wavefronts V'_A and vice versa, the influence of the wavefronts on the measured diameter therefore is based only on the difference in the path lengths in the cases B with respect to A, i.e. the diameter of the sphere itself. Therefore, when the extended DEI is used

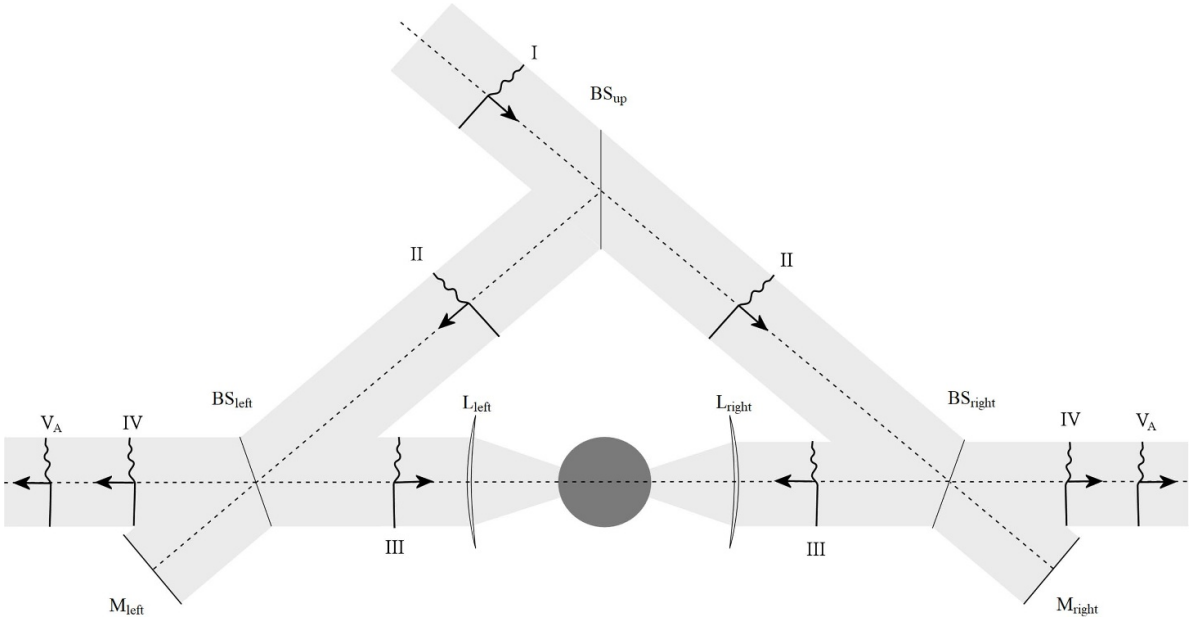

Figure 9. Propagation of a fictitious wavefront (I) in the extended DEI when a sphere is present.

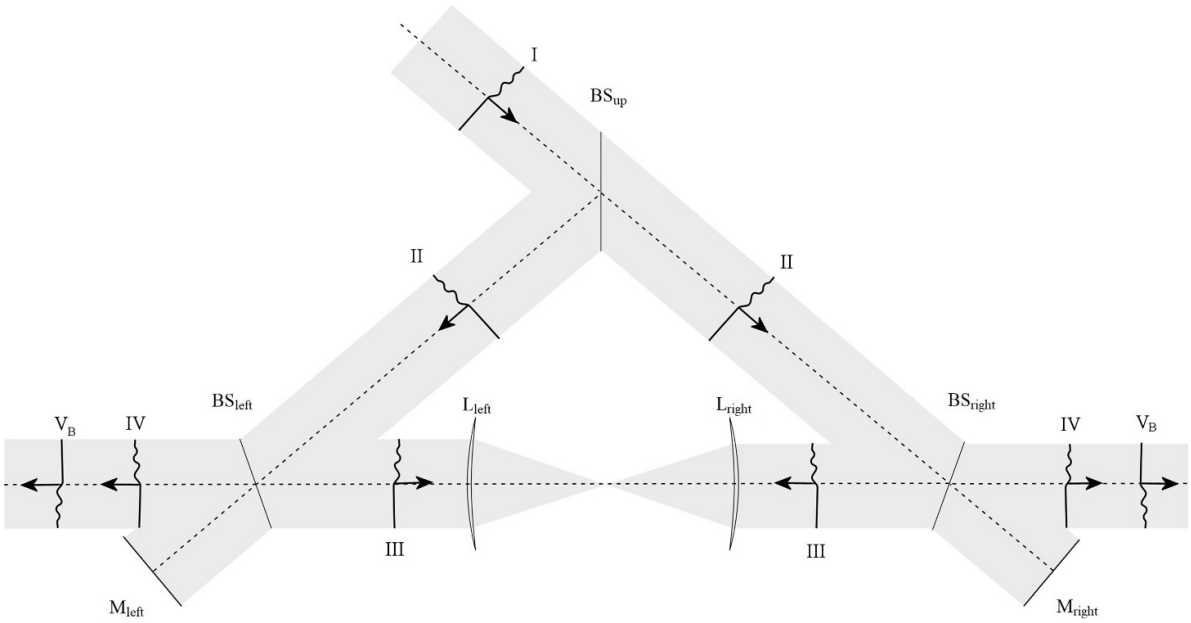

Figure 10. Propagation of a fictitious wavefront (I) in the extended DEI without inserted sphere.

to measure a diameter topography of a sphere, no additional effect of the wavefronts is expected compared to a spherical Fizeau interferometer and it can be expected that the residual effect of wavefront distortion for small spheres is negligibly small. On the other hand, the influence of wavefront distortion on the lengths differences $l_{\mathrm{B,\,left}}(x,y)$ and $l_{\mathrm{B,\,right}}(x,y)$ is obviously present when considering differences between the wavefronts V_{B} and IV in figure 10. This must be taken into account in future studies if, similarly to [20] for the spherical Fizeau interferometer, the radius topography for the extended DEI is to be derived.

4.5. Influences due to the characteristics of the spheres

As with the spherical Fizeau interferometer, only opaque spheres can be measured with the extended DEI. Otherwise, additional light transmitted through the spheres would lead to significant parasitic interference. To enable evaluable interferograms, the sphere to be measured must have an optical surface. Sphericity deviations should be resolvable with the imaging optics of the interferometer and the sphere should not have excessive scratches. Further limitations, especially regarding the attainable measurement uncertainty, arise from

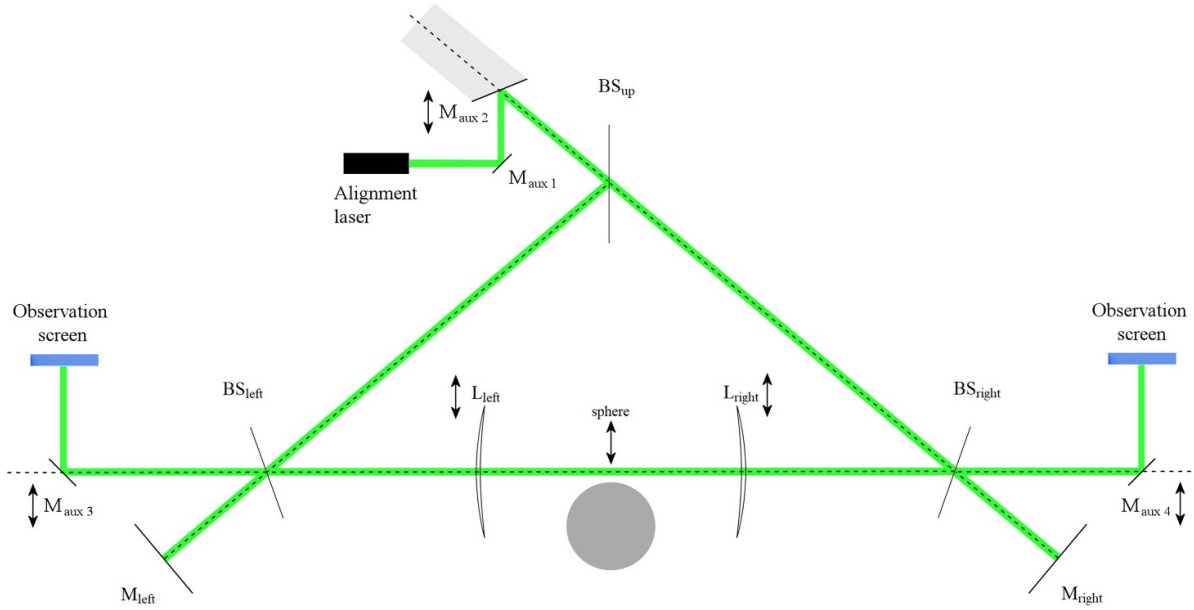

Figure 11. Adjustment setup for the extended DEI. Arrows indicate that the lenses L_{left}, L_{right}, the sphere and the mirrors $M_{aux\ 2}$ to $M_{aux\ 4}$ can be moved into and out of the beam.

surface roughness and optical phase change on reflection. Further, in the case of spheres made of ceramic materials, it can be assumed that light scattering occurs just below the (optically polished) surface, which could cause the measured diameter to be too small by up to several tens of nanometres. These effects are typically summarized in a so-called phase change correction (see [21, 22] and references therein). Therefore, the measurement and consideration of the phase change correction of the spheres is an essential prerequisite for accurate measurement of lengths.

Semi-transparent surface layers on the sphere cause the light to be reflected underneath rather than on the mechanical surface of the sphere. Apart from requiring additional knowledge about the layer thickness, multiple reflections occur within the surface layer, resulting in an additional phase shift that needs to be corrected. A prominent example for silicon spheres is given in [12], where the desired sub-nm accuracy required collecting information about the composition and thickness of multiple surface layers and calculating the influence of these layers on the measurement.

5. Proposed alignment strategy for the extended DEI

The alignment of the extended DEI first requires a suitable adjustment status of the DEI before extension, as mentioned in paragraph 2. Consequently, the lenses to be added and the sphere itself must be able to be moved into and out of the DEI via a suitable mechanism and it must be ensured that moving these assemblies does not change the status of the interferometer. Care should therefore be taken to ensure the same weight distribution within the interferometer, regardless of whether there are the lenses and/or the sphere.

Figure 11 illustrates a possible scheme for further adjustment with the inclusion of additional optical elements. First, a small beam from an alignment laser is coupled into the interferometer. Mirrors $M_{aux\ 1}$ and $M_{aux\ 2}$ are used to adjust this beam collinearly to the optical axis. While the lenses L_{left} and L_{right} are out of the beam, mirrors $M_{aux\ 3}$ and $M_{aux\ 4}$direct the beams to observation screens at the exits of the DEI. Accurate adjustment provided, a single spot is visible on each screen, which consists in two overlapping components, one from the measuring path and the other from the respective reference path. Then the first lens is moved into the beam and adjusted laterally so that on each screen the (slightly enlarged) spots from the measuring paths match their previous positions. The same procedure is performed after moving the second lens into the beam. When moving $M_{aux\ 2}$ out of the large beam, circular interference fringes should become visible on the screens and the axial distance between the two lenses is adjusted to reduce the number of fringes to a minimum. As a next step, while $M_{aux\ 2}$ is moved in again, the sphere is moved into the beam and adjusted laterally so that the corresponding spots observed on the screens again match the reference spots. Assuming that the centre position of the sphere is not too far from the focal point of the two lenses, interference fringes should be visible on the screen when moving $M_{aux\ 2}$ out of the large beam. Again, the number of fringes is adjusted to a minimum, this time by adjusting the sphere laterally and axially. Finally, the additional mirrors $M_{aux\ 3}$ and $M_{aux\ 4}$ are moved out of the beam bundle so that the interferograms can be recorded by the cameras on both sides.

The following approach can be used to determine the central pixel coordinates (x_c, y_c) that must be known in order to apply point reflection (see equation (11)). The size of an iris diaphragm used to select a small partial beam out of the collimated beam bundle is adjusted so that the beam is only

limited by it at any point in the interferometer. Thus, the visible interference in each interferogram is also limited by the iris diaphragm. If one now looks at the interferograms, which are phase-shifted with respect to one another, with regard to the intensity variation at each pixel and sets a threshold as a criterion for interference, one obtains a disk-shaped mask. The pixel coordinate of the centre of the disk, representing (x_c, y_c), can then be determined by digitally processing this mask.

6. Conclusions

Considering the simplicity of equation (9) and the described aspects of the extended DEI, the proposed extension of a DEI with two lenses for measuring spheres appears to be a promising alternative to the spherical Fizeau interferometers. While such an interferometer may react more sensitively to parameters that affect its stability due to the relatively long path lengths, the DEI offers general advantages over the spherical Fizeau interferometer. First, light sources with different laser wavelengths that are far apart can be used. This increases the unambiguity range of the interferometric diameter determinations considerably, which is particularly important for small spheres of not precisely known density, since their diameter pre-values cannot be estimated as precisely as is possible for the larger ones from the mass and known density. Second, there are more options for applying phase stepping interferometry in the DEI, e.g. by shifting the two reference mirrors. This reduces the effect of parasitic interference on the resulting phase topographies. Further, when the extended DEI is used to measure diameter topographies of spheres, there is no additional wavefront distortion effect as in a spherical Fizeau interferometer.

Currently, the DEI of PTB is on a tight schedule for its further development according to its original purpose as a gauge block interferometer. The extension presented in this paper is only planned for the next few years. In the meantime, this paper is intended to promote the idea of the extension to researchers working on existing DEIs around the world, suggesting to them a way of measuring spheres traceably. The practical implementation of this concept, possibly using the adjustment strategy proposed here, will show how precisely small spheres in particular can be measured with such an interferometer.

Data availability statement

All data that support the findings of this study are included within the article (and any supplementary files).

Acknowledgments

We would like to thank my colleagues Arnold Nicolaus, Guido Bartl and Harald Bosse (all from the PTB) as well as Professor Rainer Tutsch from the Technical University of Braunschweig for the fruitful discussions.

ORCID iD

René Schödel https://orcid.org/0000-0002-7597-9036

References

[1] BIPM 2019 The International System of Units (SI Brochure) 9th edn *Appendix 2: Practical realizations of the definitions of some important units—Mises en pratique, Mise en pratique for the definition of the metre in the SI* (available at: www.bipm.org/utils/en/pdf/si-mep/SI-App2-metre.pdf)

[2] Kuriyama Y, Yokoyama Y, Ishii Y and Ishikawa J 2006 Development of a new interferometric measurement system for determining the main characteristics of gauge blocks *Ann. CIRP* **55** 563–6

[3] Abdelaty A, Walkov A, Franke P and Schödel R 2012 Challenges on double-ended gauge block interferometry unveiled by the study of a prototype at PTB *Metrologia* **49** 307–14

[4] Buchta Z, Řeřucha Š, Hucl V, Čížek M, Šarbort M, Lazar J and Číp O 2013 Active angular alignment of gauge blocks in double-ended interferometers *Sensors* **13** 13090–8

[5] Kruger O, Hungwe F, Farid N and Schreve K 2014 The design of a double-ended interferometer (DEI) *Int. J. Metrol. Qual. Eng.* **5** 408

[6] Byman V and Lassila A 2015 MIKES' primary phase stepping gauge block interferometer *Meas. Sci. Technol.* **26** 084009

[7] Saunders J B 1972 Ball and cylinder interferometer *J. Res. Nat. Bur. Stand.* **76C** 11–20 (https://nvlpubs.nist.gov/nistpubs/jres/76C/jresv76Cn1-2p11_A1b.pdf)

[8] Peuto A, Sacconi A, Panciera R, Pasin W and Rasetti M 1984 Precision measurements on solid artifacts for a redetermination of the density of water *Precision Measurement and Fundamental Constants II* NBS Special Publication ed B N Taylor and W D Phillips 11 (Washington, DC: Natl Bur Stand (U.S.), Spec.Publ.) vol 617 pp 449–52 (https://nvlpubs.nist.gov/nistpubs/Legacy/SP/nbsspecialpublication617.pdf)

[9] Leistner A and Zosi G 1987 Polishing a 1-kg silicon sphere for adensity standard *Appl. Opt.* **26** 600–1

[10] Kuramoto N and Fujii K 2009 Improvement in the volume determination for Si spheres with an optical interferometer *IEEE Trans. Instrum. Meas.* **58** 915–8

[11] Nicolaus A and Bönsch G 1998 Doppelseitige Fizeau-Interferometer mit Phasenverschiebeauswertung für dimensionelle Messungen *Tech. Mess.* **65** 83–9

[12] Bartl G, Bettin H, Krystek M, Mai T, Nicolaus A and Peter A 2011 Volume determination of the Avogadro spheres of highly enriched 28Si with a spherical Fizeau interferometer *Metrologia* **48** S96–103

[13] Mai T and Nicolaus A 2017 Optical simulation of the new PTB sphere interferometer *Metrologia* **54** 487–93

[14] BIPM 2019 The International System of Units (SI Brochure) 9th edn (available at: www.bipm.org/en/publications/si-brochure/)

[15] BIPM 2019 The International System of Units (SI Brochure) 9th edn *Appendix 2: Practical realizations of the definitions of some important units—Mises en pratique* (available at: www.bipm.org/en/publications/mises-en-pratique/)

[16] Rau K and Schödel R 2014 Double-ended interferometer for measuring gauge blocks without wringing *Fringe 2013: 7th Int. Workshop on Advanced Optical Imaging and Metrology* pp 859–62

[17] Skupin K 2020 Absolute Längenmessung prismatischer Körper mit dem beidseitig antastenden Interferometer der PTB PhD Thesis (https://doi.org/10.18452/21614)

[18] Fischedick M, Bartl G and Schödel R Beidseitig optisch antastendes Interferometer zur Längenmessung von Endmaßen ohne Anschub *DGaO-Proc. 2018* (available at: www.dgao-proceedings.de/download/119/119_p8.pdf)
[19] Schödel R 2015 Utilisation of coincidence criteria in absolute length measurements by optical interferometry in vacuum and in air *Meas. Sci. Technol.* **26** 084007
[20] Bartl G, Krystek M and Nicolaus A 2014 PTB's enhanced stitching approach for the high-accuracy interferometric form errorcharacterization of spheres *Meas. Sci. Technol.* **25** 064002
[21] Lassila A and Byman V 2015 Wave front and phase correction for double-ended gauge block interferometry *Metrologia* **52** 708–16
[22] Balling P, Ramotowski Z, Szumski A, Lassila A, Křen P and Mašika P 2019 Linking the optical and the mechanical measurements of dimension by a Newton's rings method *Metrologia* **56** 025008